Developments in Environmental Science, Volume 5
D. Sarkar, R. Datta and R. Hannigan (Editors)

ISSN: 1474-8177/DOI:10.1016/S1474-8177(07)05020-6

Chapter 20

Understanding spatial variability and its application to biogeochemistry analysis

Sabine Grunwald, Rosanna L. Rivero and K. Ramesh Reddy

Abstract

Transforming the conceptual ideas of biogeochemical cycling into spatially explicit context has been hampered by ecosystem complexity, multiple nested levels of interrelated physical, biological and chemical processes, and the lack of sufficient quantitative data. The mosaic of ecosystem structures and functions distributed across a landscape represent the combined effects and interactions of a variety of biotic and abiotic factors. As a result, existing landscape patterns implicitly contain information about the processes that generated these patterns. Deductive science has generated extensive knowledge of how individual parts of aquatic ecosystem's function derived from site-specific studies. Yet, understanding of how the parts interact as a whole requires a holistic perspective that considers the spatial variability, distribution and interaction of all components of a landscape. The predicament entailed by the complexity of aquatic ecosystems requires a synergistic approach that integrates knowledge from different disciplines including biogeochemistry, geography, statistics/geostatistics, ecology, hydrology and others. Interdisciplinary collaboration will be key to reconcile deductive and inductive science and allow us to understand the linkages between biogeochemical properties and processes at landscape scale. In this chapter we provide an overview of a variety of geostatistical and hybrid methods that can be used to characterize the spatial variability, distribution and uncertainty of biogeochemical properties. A case study demonstrates the application of these methods to predict soil total phosphorus across a wetland in the Greater Everglades.

20.1. Introduction

Conceptually, scale represents the *window of perception*, the filter, or the measuring tool through which a landscape may be viewed or perceived (Levin, 1992). Thus, changing the scale changes the properties that we observe—the patterns of reality, which has implications for understanding the dynamics of any environmental system. Since parameters and processes important at one scale are frequently not important or predictive at another, it is essential to gain a better understanding of the spatial variability and distribution of ecosystem properties. Turner et al. (1989) pointed out that ecological problems often require the upscaling of fine-scale measurements for the analysis of coarse-scale phenomena. A holistic view of landscapes is required to understand ecosystem processes at micro, meso and macro spatial scales.

Biogeochemistry is defined as the scientific study of the interactions among the biological, geological and chemical systems of Earth, including the cycling of matter and energy through them. Numerous conceptual models have been developed that describe the cycling of matter and material in aquatic ecosystems (Mitsch and Gosselink, 2000). The carbon (C), nitrogen (N), phosphorus (P) cycles play a critical role in the functioning of wetland ecosystems, their structure, resilience and sensitivity to natural and human-induced disturbances.

In this chapter we discuss the importance of spatially explicit mapping of biogeochemical properties that applies to aquatic and terrestrial ecosystems in the context of spatial autocorrelation and covariation of these properties. Understanding the spatial variability and distribution of biogeochemical properties is a necessity for holistic assessment of environmental quality at landscape-scale.

20.2. Concepts and methods

The mosaic of system structures and functions distributed across a landscape represent the combined effects and interactions of a variety of biotic and abiotic factors. As a result, existing landscape patterns implicitly contain information about the processes that generated these patterns (Holling and Gunderson, 2002). Spatial and temporal ecosystem attributes are neither uniform nor scale independent. Likewise, biogeochemical properties and processes vary gradually and continuously in space and time. Discrete boundaries that cause abrupt shifts from high to low values of physico-chemical and biological properties are limited to crisp physical boundaries (e.g., hydrologic boundaries, land use) or

anthropogenic disturbances. To restrict observations to few sites (e.g., along a transect) limits the ability to capture the biogeochemical signatures of a landscape.

Some biogeochemical properties are labor-intensive and costly to derive (e.g., phosphorus fractionation schemes, alkaline phosphatase activity) whereas other measurements are standard routine (e.g., bulk density, total phosphorus—TP). Hence, in the past, numerous studies focused on sparse spatially distributed sampling or experimental lab/field studies to understand biogeochemical cycling (Reddy et al., 1998; White and Reddy, 2000; Fisher and Reddy, 2001; Craft and Chiang, 2002; Karathanasis et al., 2003; Morris et al., 2004) resulting in a tremendous amount of knowledge. The strength of such site-specific studies is to describe feedback processes in response to a localized change in biogeochemical conditions. For example, changing plant communities provide feedback on soil biogeochemical properties and microbial communities that respond to changing environmental conditions (e.g., organic matter, hydroperiod, temperature, light, etc.). Numerous site-specific studies have ignored the *spatial* interrelationships, i.e., the *spatial covariation*, among different biogeochemical properties and assume independence of observations. Deductive science has generated extensive knowledge of how individual parts of aquatic ecosystems function (compare Eq. (1)). Yet, understanding of how the parts interact as a whole requires a holistic perspective that considers the spatial interaction of all components of a landscape. Transforming the conceptual ideas of biogeochemical properties and processes into spatially explicit context has been hampered by ecosystem complexity, multiple nested levels of interrelated physical, biological and chemical processes, and the lack of sufficient quantitative data.

$$y(x_i) = f\{z_j(x_i)\} \tag{1}$$

where $y(x_i)$ is the response variable observed at location x_i and $z_j(x_i)$ the biogeochemical properties ($j = 1, 2, 3, \ldots, n$) observed at location x_i.

20.2.1. The concept of spatial autocorrelation

The deductive approach is rooted in the concept developed by Fisher (1925), who pointed out the importance of random selection ensuring that estimates are unbiased. This assumption of independence is a prerequisite for many statistical tests including regression analysis, analysis of variance, *t*-tests and others (Berthouex and Brown, 2002). Classical statistical methods have been used extensively to document significant differences in biogeochemical properties/behavior using controlled experiments (e.g., mesocosms), plots, or blocks. Such analyses are based on the assumption

that the investigated properties show no spatial autocorrelation. *Spatial autocorrelation* is a term referring to the degree of relationship that exists between two or more spatial variables, such that when one changes, the other(s) also change (Webster and Oliver, 2001). This change can either be in the same direction, which is a positive autocorrelation, or in the opposite direction, which is a negative autocorrelation (Burrough, 1986; Isaaks and Srivastava, 1989). Popular measures of spatial autocorrelation are Moran's I (Moran, 1950) and Geary's C (Geary, 1954) coefficients. Positive values of Moran I and value smaller than 1 for Geary's C coefficient correspond to positive autocorrelation. True spatial independence of properties in aquatic and terrestrial landscapes does not really exist due to the interconnectedness of biogeochemical processes of N, C and P and other nutrients and transport processes that move water, material and energy through the ecosystem. Rather, the sampling density and spacing between observations determine if the underlying spatial autocorrelation can be captured by a model or not. Studies that limit observations to sparse sampling locations far apart from each other ignore spatial autocorrelation and focus on the identification of significant differences between sites with contrasting biogeochemical conditions. However, numerous studies documented that spatial autocorrelation of biogeochemical soil properties is inherent at landscape scale [$> 1\,km^2$] (Newman et al., 1997; DeBusk et al., 2001; Grunwald et al., 2004, 2006; Bruland and Richardson, 2005). To identify spatial autocorrelation of a specific biogeochemical property, observations need to be collected with a spatially distributed design throughout an ecosystem that accounts for short-, medium- and long-range variability. Constraining biogeochemical observations to few point locations (sites) cannot possibly explain the underlying spatial autocorrelation of properties as well as interrelationships between different biogeochemical properties (e.g., TP and labile P), which is called the spatial covariation. The predicament entailed by the complexity of aquatic and terrestrial ecosystems requires a synergistic approach integrating knowledge from different disciplines including biogeochemistry, geography, statistics/geostatistics, ecology, hydrology and others. Interdisciplinary collaboration will be key to reconcile deductive and inductive science to understand the linkages between properties and processes at landscape scale. Each soil biogeochemical property exhibits specific behavior of spatial autocorrelation that is related to environmental factors such as nutrient cycling, hydrology, topography, anthropogenic-induced nutrient inputs, vegetation types, etc. and spatial scale. For example, TP showed long-range correlation lengths across the Water Conservation Area-2A (WCA-2A), a wetland in the northern Everglades, in 1990 and 1998 with spatial autocorrelations of 6500 and

7549 m, respectively (Grunwald et al., 2004). Similar long-range spatial autocorrelation for TP was found in the Blue Cypress Marsh Conservation Area, a wetland in eastern Florida, with 7240 m (Grunwald et al., 2006).

20.2.2. The concept of regionalized variable theory

We can formalize the concept of spatial variation outlined above using the theory of regionalized variables (Webster and Oliver, 2001). Since the environment and its component attributes result from many interactive physical, chemical and biological processes that are non-linear and/or chaotic, the outcome is so complex that the variation appears to be random. If we adopt a stochastic view then at each point in geographic space there is not just one value for an attribute but a whole set of values. Consider a region R that comprises an infinite number of points x_i, $i = 1$, 2, …, ∞. Whereas in the classical statistical approach the values of an observed biogeochemical attribute, z, at these points constitute the population, in the geostatistical approach this population is assumed to be just one realization of a random process or random function that could generate any number of such populations. Then, at each place x_0 the attribute is considered a random variable $Z(x_0)$. Thus, at a location x_0 a biogeochemical attribute is treated as a random variable with mean (μ), a variance ($\sigma 2$) and a cumulative distribution function (cdf). Note, that the actual value $z(x_0)$ is just one drawn at random from that distribution. The set of random variables, $Z(x_1)$, $Z(x_2)$, … $Z(x_n)$ constitute a random function or a stochastic process (Webster and Oliver, 2001). Regionalized variable theory assumes that the spatial variation of any biogeochemical variable can be expressed as the sum of three major components (Eq. (2)) (Burrough and McDonnell, 1998): (i) a structural component having a constant mean or trend that is spatially dependent, (ii) a random, but spatially correlated component, known as the variation of the regionalized variable and (iii) a spatially uncorrelated random noise or residual term. A non-stationary trend extends over the whole study area and is therefore called a global model. In contrast, local trends, also called drift, describe localized variation (Webster and Oliver, 2001). [Note: a header "$\hat{Z}$" indicates that the variable is estimated]

$$\hat{Z}(x_i) = m(x_i) + \varepsilon'(x_i) + \varepsilon'' \tag{2}$$

where $\hat{Z}(x_i)$ is the value of a random variable at locations x_i with $i = 1$, $2, \ldots, n$; $m(x_i)$ the trend model—deterministic function describing the "structural" component of $\hat{Z}(x_i)$; $\varepsilon'(x_i)$ the stochastic, locally varying but spatially dependent component (the regionalized variable); ε'' the A

residual, spatially independent noise term having zero mean and variance; and x_i the geographic position in 1, 2 or 3 dimensions.

Observations obtained close to each other are more likely to be similar than observations taken further apart from each other. This spatial correlation of $\varepsilon'(x_i)$ is described by the semivariance $\hat{\gamma}(h)$ (Eq. (3)). If γ is plotted as a function of the lag distance h that separates x_i and x_i+h, the semivariogram is obtained. One implicit assumption is that the mean, variance and covariance depend only on the separation distance h and not on the absolute position. This assumption constitutes second-order stationarity (Isaaks and Srivastava, 1989). $\hat{\gamma}(h)$ is estimated as

$$\hat{\gamma}(h) = \frac{1}{2N(h)} \sum_{i=1}^{N(h)} [z_u(x_i) - z_u(x_i + h)]^2 \tag{3}$$

where $\hat{\gamma}(h)$ is the semivariance at lag h; h the distance between data pairs ($z_u(x_i) - z_u(x_i+h)$) (or lag); N the total number of data pairs ($z_u(x_i) - z_u(x_i+h)$); and $z_u(x_i)$ the biogeochemical variable u.

Commonly, least square fitting of the experimental semivariogram model is used. However, visual inspection of the statistical fitting process is essential. Alternatively, interactive fitting can be used to model the semivariogram. Characteristic parameters that can be derived from semivariograms are the *nugget*, *sill* and *range*. The nugget describes the measurement error and fine-scale variability. Semivariograms of properties or processes that exhibit second-order stationarity reach upper bounds at which they remain after their initial increases. This upper bound, or maximum is known as the sill. The range describes the spatial autocorrelation and marks the limit of spatial dependence (Webster and Oliver, 2001). The univariate semivariance can be extended to consider two biogeochemical variables, z_u and z_v, to derive the cross-semivariances $\hat{\gamma}_{uv}(h)$.

$$\hat{\gamma}_{uv}(h) = \frac{1}{2N(h)} \sum_{i=1}^{N(h)} [z_u(x_i) - z_u(x_i + h)][z_v(x_i) - z_v(x_i + h)] \tag{4}$$

Regionalized variable theory and semivariogram analyses are described in detail by Goovaerts (1997), Chilès and Delfiner (1999), Webster and Oliver (2001, 2005). The semivariogram provides input for kriging, which is a weighted interpolation technique to create continuous prediction maps of biogeochemical properties. Major limitations of the univariate geostatistical technique of kriging are due to the assumption of stationarity, which is often not met by the field-sampled datasets and the large amount of data (>100 observations; recommended >150 observations)

required to characterize the spatial autocorrelation of a property (Webster and Oliver, 2001).

20.2.3. Global models

Global models use all available observations to provide predictions for the whole area of interest, while local interpolators operate within a small zone around the point being interpolated to ensure that estimates are made only with data from locations in the immediate neighborhood (Burrough and McDonnell, 1998). Trend surfaces are the simplest global, geospatial model that requires fitting some form of polynomial equation through biogeochemical attribute values. These are least square methods that model the long-range spatial variation. Such models assume that the spatial coordinates are the independent variables and z (attribute of interest) is the dependent variable (Webster, 1994). As trend surfaces are simplified representations of reality, it is difficult to ascribe any physical meaning to complex, higher-order polynomials. Therefore, the main use of trend surface analysis is not as an interpolator, but as a way of removing broad features of the data prior to using some complex local interpolator. The concept is based on partitioning the variance between trend and the residuals from the trend. Compare Eq. (2) that partitions the variability of a property into (i) a global trend component, (ii) stochastic, locally varying but spatially dependent component and (iii) a residual noise term.

20.2.4. Local models

Local, deterministic interpolation methods focus on modeling short-range local variations. The interpolation involves: (i) defining a search neighborhood around the point to be interpolated, (ii) finding the observations within this neighborhood, (iii) choosing a mathematical function to represent the variation over this limited number of points or area, and (iv) evaluating it for the point on a regular grid. The procedure is repeated until all the points on a grid have been computed (Burrough and McDonnell, 1998). For example, commonly used local interpolation methods are inverse distance weighting (IDW), splines and kriging (Burrough and McDonnell, 1998). Splines (local fitting functions) estimate values using a mathematical function that minimizes overall surface curvature, resulting in a smooth surface that passes exactly through the observation points, while at the same time ensuring that the joins between one part of the curve (or surface) and another are continuous. In contrast to trend surfaces and weighted averages, splines retain small-scale

features. A disadvantage of splines and IDW is that there are no direct estimates of the errors associated with these forms of interpolation (Burrough and McDonnell, 1998). Local interpolators in its simplest form are based weights that are computed from a linear function of distance between sets of data points and the point to be predicted (Eq. (5)).

$$\hat{Z}(x_0) = \sum_{i=1}^{n} \lambda_i * z(x_i) \quad \sum_{i=1}^{n} \lambda_i = 1 \tag{5}$$

where $\hat{Z}(x_0)$is the predicted attribute value at unsampled location x_0; λ_i the weights; $z(x_i)$ the observed attribute value at locations x_i; and n the number of observations.

In Eq. (5) $z(x_1)$, $z(x_2)$, … $z(x_n)$ are the measured values of the biogeochemical property z at locations x_1, x_2, …, x_n and λ_i are the weights that sum to 1 to assure unbiasedness. The expected error is $E[\hat{Z}(x_0) - Z(x_0)] = 0$ and the prediction variance is

$$\begin{aligned} \text{var}[\hat{Z}(x_0)] &= E[\{\hat{Z}(x_0) - Z(x_0)\}^2] \\ &= 2\sum_{i=1}^{N} \lambda_i \gamma(x_i, x_0) - \sum_{i=1}^{N}\sum_{j=1}^{N} \lambda_i \lambda_j \gamma(x_i; x_j) \end{aligned} \tag{6}$$

where $\gamma(x_i; x_0)$ is the semivariance of Z between the ith sampling point and the target point x_0 at an unsampled location and $\gamma(x_i; x_j)$ the semivariance of Z between sampling points x_i and x_j.

20.2.5. Kriging

Kriging is a generic term adopted by geostatisticians for a family of generalized least-squares regression algorithms. In the kriging system the goal is to minimize the kriging variance, where the weights sum to 0 (Eq. (7)).

$$\sum_{i=1}^{n} \lambda_i(x_i; x_j) - \psi(x_0) \text{ with } \sum_{i=1}^{n} \lambda_i = 0 \tag{7}$$

where $\psi(x_0)$ is the Lagrange multiplier.

All kriging estimators are but variants of the basic linear regression estimator $\hat{Z}(x_0)$ defined as

$$\hat{Z}(x_0) - m(x_0) = \sum_{i=1}^{n} \lambda_i(x_0)[Z(x_i) - m(x_i)] \tag{8}$$

where $\hat{Z}(x_0)$ is the linear regression estimator at unsampled location x_0 and $\lambda_i(x_0)$ the weights assigned to datum x_0 interpreted as a realization of

the random variable $Z(x_i)$ and located within a given neighborhood $W(x)$ centered on x.

The weights are chosen to minimize the error variance $\sigma 2(x_0) = \text{var}\{\hat{Z}(x_0) - Z(x_0)\}$ under the constraint of unbiasedness of the estimator. These weights are obtained by solving simultaneously a system of linear equations which is known as the kriging system (Goovaerts, 1999).

The local neighborhood characteristics including (i) the number of observations ($z(x_i)$) within a neighborhood, (ii) major and minor semiaxis (size of the neighborhood) and (iii) the neighborhood shape (uniform or discretized into subunits) determine the strengths of smoothing. In general, a small neighborhood generates localized predictions based on few observations, which are prone to the influence of extreme values producing blocky/crisp looking maps. In contrast, large neighborhoods smooth over a larger area providing conservative predictions for areas with high observed values.

20.2.6. Kriging variants

Differences in kriging variants reside in the model considered for the trend $m(x)$ (Goovaerts, 1999):

(a) *Simple kriging* (*SK*) considers the mean $m(x)$ known and constant throughout the study area.
(b) *Ordinary kriging* (*OK*) accounts for local fluctuations of the mean by limiting the domain of stationarity of the mean to the local neighborhood ($W(x)$). The mean is considered constant but unknown.
(c) *Universal kriging* (*UK*), also known as kriging with a trend model, considers that the unknown local mean $m(x')$ smoothly varies within each local neighborhood, and the trend is modeled as a linear combination of functions $f_k(x)$ of the coordinates

$$m(x') = \sum_{k=0}^{K} a_k(x') f_k(x') \tag{9}$$

with $a_k(x')$ constant within each local neighborhood $W(x)$ but unknown.
(d) *Regression kriging* (*RK*): Alternatively, the trend function $m(x)$ can be modeled separately, where kriging is combined with regression or a regression variant (Odeh et al., 1994, 1995; Odeh and McBratney, 2000; Hengl et al., 2004). The deterministic component $m(x)$ is considered dependent on some exogenous factors such as climate, hydrology, topography, vegetation or other environmental factors that can be described via multivariate regression, Generalized Linear

Models, Classification and Regression Trees, Generalized Additive Models or other functions. Odeh et al. (1994, 1995) defines regression kriging where model $f(.)$ is used to describe the relationship between predictors and environmental factors:

$$\hat{Z}(x_i) = f(Q, x_i) + \hat{R}(x_i) \tag{10}$$

where $f(Q,\ x_i)$ is the function describing the structural component of $\hat{Z}(x_i)$as a function of Q environmental variables at location x_i; $\hat{R}(x_i)$ the stochastic, locally varying but spatially dependent residual from $f(Q,\ x_i)$. In RK, the target biogeochemical property at an unvisited site is first predicted by $f(.)$, followed by kriging of the residuals of the model.

(e) *Kriging with an external drift* (*KED*) models the trend $m(x)$ as a linear function of a smoothly varying secondary (external) variable $y(x)$ instead of a function of the spatial coordinates. Besides the difficult inference of the residual semivariogram, this method requires that the relation between the primary trend and secondary variable is linear and makes physical sense (Goovaerts, 1999). In KED the secondary exhaustive data are only used to inform on the shape of the trend of the primary variable. In contrast, cokriging exploits more fully the secondary information by directly incorporating the values of the secondary variable and measuring the degree of spatial association with the primary variable through the cross-semivariogram. Cokriging is the extension of ordinary kriging of a single variable to two or more variables. There must be some kind of coregionalization among the variables for it to be profitable. It is particularly useful if some property that is cheap to measure (e.g., remote sensing image) is spatially correlated with another property that is expensive to measure and/or labor intensive to collect and available at few sites (Webster and Oliver, 2001).

In many environmental applications a few hot spots (high values) coexist with many small values that vary continuously in space. Depending on whether large values are clustered or scattered in space, our physical interpretation of the biogeochemical processes controlling high and low values may change. The characterization of the spatial distribution of z-values above or below a given threshold value z_k requires prior coding of each observation as an indicator datum *ind* $(x_i;\ z_k)$ defined as (Goovaerts, 1999):

$$\begin{aligned} ind(x_i; z_k) &= 1 \quad \text{if } z(x_i) \le z_k \\ &= 0 \quad \text{otherwise} \end{aligned} \tag{11}$$

Indicator semivariograms can be computed by substituting indicator data *ind* $(x_i; z_k)$ for z-data:

$$\hat{\gamma}(h, z_k) = \frac{1}{2N(h)} \sum_{i=1}^{N(h)} [ind(x_i; z_k) - ind(x_i + h; z_k)]^2 \qquad (12)$$

The indicator variogram value $\hat{\gamma}(h, z_k)$ measures how often two z-values separated by a vector h are on opposite sides of the threshold value z_k.

20.2.7. Spatial stochastic simulations

Least-square interpolation algorithms such as kriging tend to smooth out local details of the spatial variation of the attribute, with small values typically overestimated and large values underestimated (Isaaks and Srivastava, 1989). This is a serious shortcoming if large pollutant concentrations or biogeochemical property values are of interest.Kriging aims at local accuracy through minimizing a covariance-based error variance, while spatial stochastic simulation aims at reproducing spatial structure through a covariance model. Unlike kriging, spatial conditional stochastic simulations do not aim at minimizing a local error variance but focus on the reproduction of statistics such as the sample histogram or the semivariogram model in addition to honoring of data values. The output results, i.e., a set of alternative realizations, provide a visual and quantitative measure of the spatial uncertainty. A probability distribution (ccdf) for attributes at a particular location can be built for a set of multiple realizations of the joint distribution of attribute values in space (Goovaerts, 1997). Kriging produces one output map. In contrast, stochastic simulation generates multiple realizations of the spatial distribution of (biogeochemical) attribute values and it uses differences among simulated maps as a measure of uncertainty. Therefore, kriging is preferred for local estimation whereas simulation is increasingly preferred for assessment of spatial uncertainty and reproduction of global statistics, risk assessment, flow modeling and water quality simulation modeling (Goovaerts, 1997; Grunwald et al., 2004; Chilès and Allard, 2005). The latter situations require knowledge about the uncertainty of environmental attribute values at many locations simultaneously (multiple-point or spatial uncertainty).

Conditional Sequential Gaussian Simulation (CSGS) is a stochastic simulation method for the generation of partial realizations using normal random functions. The method uses the Gaussian model type and is ergodic, which means that simulations have a sample mean close to the theoretical mean and a sample covariance to the theoretical covariance

$C(h)$. This implies that all simulations are drawn from the realizations of a random function that is ergodic in the mean value and the covariance (second-order ergodicity) (Chilès and Delfiner, 1999). Conditioning is the operation that ensures that simulation values match values at sample points. Conditional Sequential Gaussian Simulation provides a measure of local uncertainty because each conditional cdf relates to a single spatial location x.

20.2.8. Summary

A flow chart that provides an overview of statistical, geostatistical and hybrid geospatial modeling techniques presented above is shown in Fig. 20.1. Depending on the spatial autocorrelation and the spatial covariation, different methods are suggested to generate the best possible predictions of biogeochemical properties within a given aquatic ecosystem. Many variations of these methods exist that can be further explored in Goovaerts (1997), Webster and Oliver (2001, 2005), McBratney et al. (2000, 2003) and Grunwald (2005).

20.3. Case study

In this case study we illustrate the concepts and methods outlined above to characterize spatial variability of TP within a subtropical wetland, WCA-2A, located in the Greater Everglades, Florida. The Everglades is a naturally P-limited aquatic ecosystem that has been impacted by nutrient inputs from agricultural land use over the last decades (Noe et al., 2001). In addition, this system has been manipulated hydrologically (canals, levees, hydrologic control structures) altering the historic uninterrupted sheet flow through the whole system (Porter and Porter, 2002). Water Conservation Area-2A is 418 km^2 in size consisting primarily of Histosols (soils with at least 12–18% organic C by weight), which developed during the past 5000 years (McCollum et al., 1976). Vegetative communities are dominated by sawgrass (*Cladium jamaciense Crantz*), cattail (*Typha spp.*), mixed sawgrass and cattail communities and few tree islands (Porter and Porter, 2002). The wetland is surrounded by canals and levees with two major surface water inflow points (S-7 and S-10 pump stations). Water moves through WCA-2A as sheet flow from the north-east to the outflow located south (DeBusk, 2001). Elevated soil P concentration in WCA-2A has been strongly linked to productivity and community structure of macrophytes (McCormick et al., 2002).

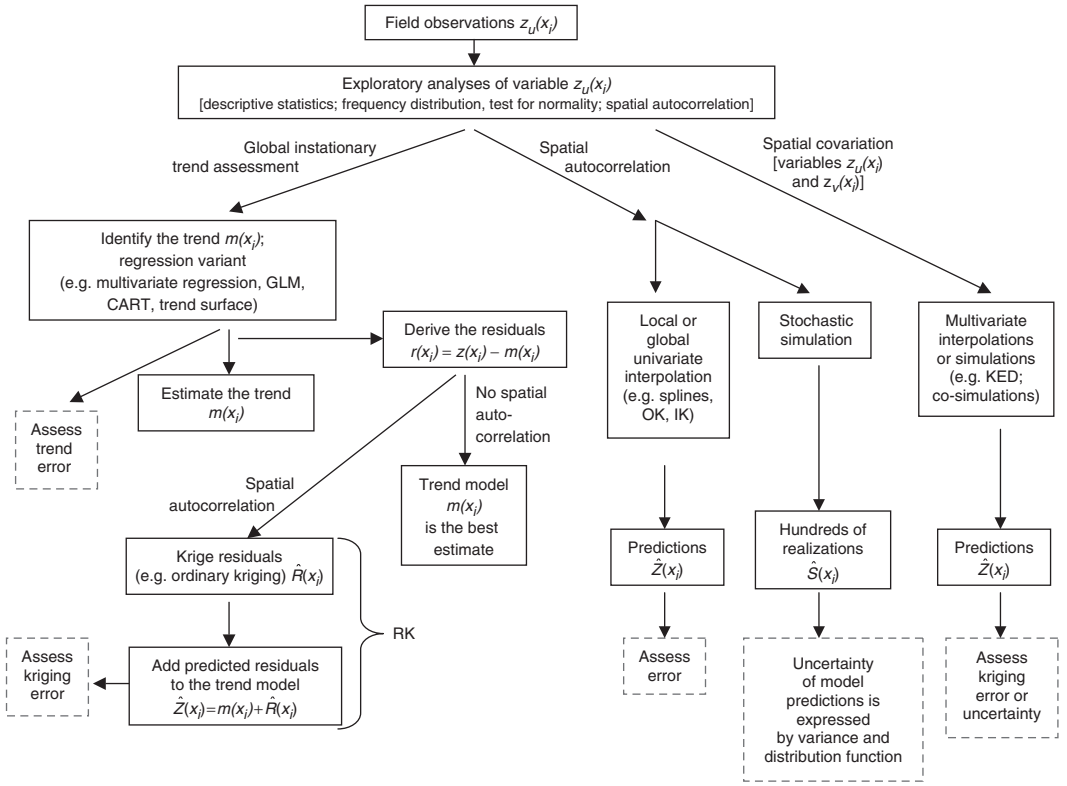

Figure 20.1. Decision flowchart for spatial modeling of biogeochemical soil properties.

In 2003, we collected soil samples at 0–10 cm depth at 111 sites based on a stratified random sampling design, spatially distributed throughout WCA-2A that were analyzed for TP. Strata were derived using historic ecological data layers such as the Normalized Difference Vegetation Index as a proxy for vegetative communities, as well as soil and hydrologic data. The sampling design was optimized to account for short-, medium- and long-range variability of attributes. A map that shows the distribution of soil observations is shown in Fig. 20.2. Total P was measured with a dry ashing procedure (Anderson, 1976) followed by determination with an automated colorimetric procedure (U.S. Environmental Protection Agency, 1993, Method 365.1). We complemented the soil dataset with an exhaustive ancillary dataset derived from Advanced Spaceborne Thermal Emission and Reflection Radiometer (ASTER) satellite image. The ASTER sensor covers a wide spectral range and high spatial and radiometric resolutions. The spectral region is covered by three telescopes, three Visible and Near Infrared Radiometer (VNIR) bands with a spatial resolution of 15 m, six Short Wave Infrared Radiometer (SWIR) bands with a spatial resolution of 30 m and five thermal Infrared Radiometer (TIR) bands with a spatial resolution of

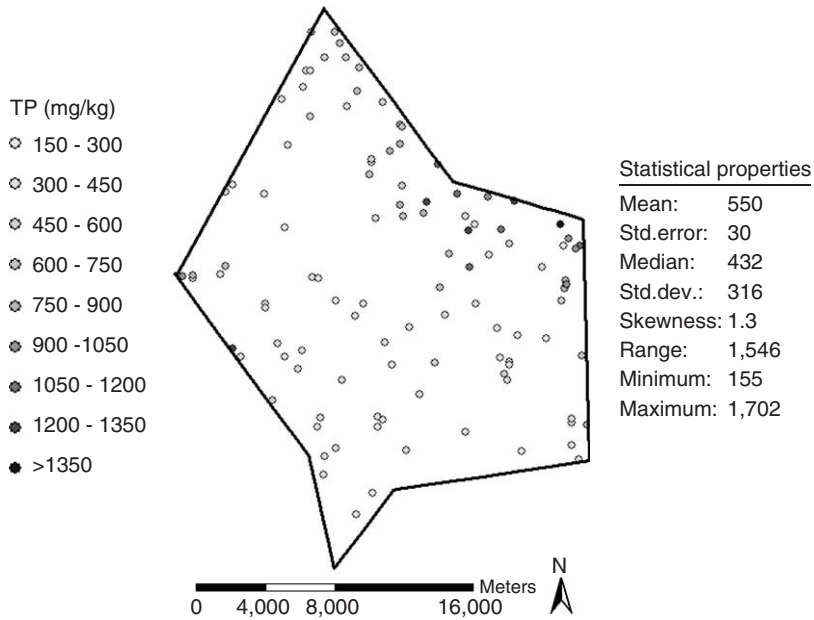

Figure 20.2. Observations of total phosphorus (TP) at 0–10 cm depth measured at 111 locations across WCA-2A.

90 m (Abrams et al., 2002). For the purpose of this study, we used ASTER bands 2 and 3 (red and near-infrared) from the VNIR spectral region in order to calculate the Normalized Difference Vegetation Index (NDVI) (Rouse et al., 1974), which is slightly different when compared to the NDVI derived from Landsat satellite images that use bands 3 and 4.

Descriptive statistics of TP are enclosed in Fig. 20.2 and indicate a positively skewed distribution with a skewness coefficient of 1.3, mean of 550, median of 432, minimum of 155 and maximum of 1702 mg kg^{-1}. To predict TP across the WCA-2A we used completely regularized splines with different neighborhood options (Fig. 20.3). The spline map in Fig. 20.3c shows the smoothing effect of using a large local neighborhood with 15 observations (minimum of 5) to predict TP at unsampled locations. In contrast, spline map 1 (Fig. 20.3a) shows blocky spatial patterns due to the small local neighborhood with few (6) observations (minimum of 2) that contributed to the predictions of TP at unsampled locations. The mean prediction error for was lowest for spline map 2 with 0.4688, followed by spline map 3 with −3.631 and spline map 1 with −4.598. The RMSE was similar for spline map 3 with 252 and spline map 2 with 253 and highest for spline map 1 with 293. Here, a heuristic approach was used to identify the interpolation method that showed the lowest prediction errors.

To explore the spatial autocorrelation of TP, h-scattergrams and semivariograms were generated (Fig. 20.4). Just as the scattergram is a plot of all pairs of values related to two different attributes measured at the same location, the h-scattergram is a plot of all pairs of measurements ($z(x_i)$, $z(x_i+h)$) on the same attribute z at locations separated by a given distance h in a particular direction. A perfect correlation would entail that all points in the h-scatter diagram lie on the line of equal values. As seen in Fig. 20.4, the spread of the points indicated the variability of TP values. The increasing inflation of the cloud in all h-scattergrams computed in four different directions reflected the increasing dissimilarity between observations farther apart. Overall, no distinct different patterns in the directional h-scatter diagram were found indicating isotropic spatial distributions. Isotropic means that the spatial patterns are the same/similar in different directions.

Because the TP data were non-Gaussian we transformed TP values with a log transformation to approximate a normal distribution. The omnidirectional experimental semivariogram of log TP is shown in Fig. 20.4b that was fitted with an exponential model with a nugget of 0.0185, sill 0.0512 and range of 7468 m. At the range the spatial autocorrelation becomes 0 indicating that this separation distance h marks the limit of spatial dependence. Observations taken further apart than the

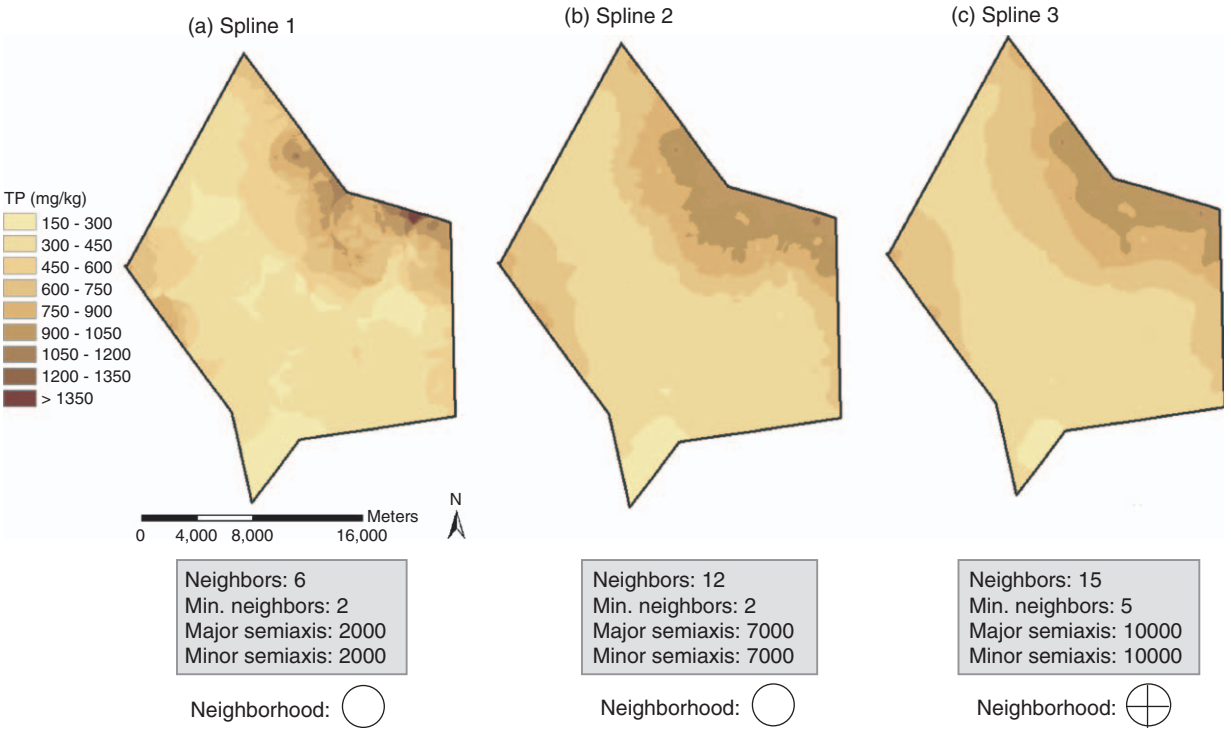

Figure 20.3. Predictions of TP derived from Completely Regularized Splines with different local neighborhood options.

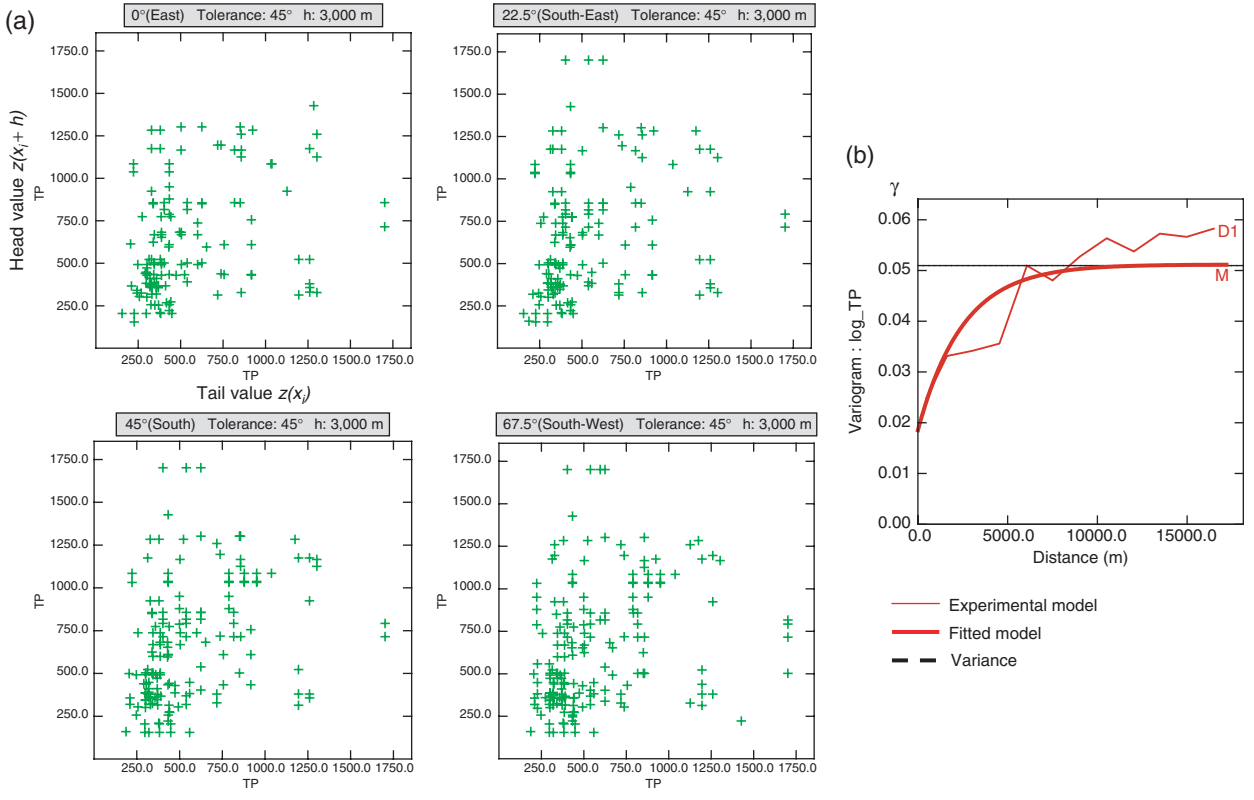

Figure 20.4. (a) h-scattergrams and (b) semivariogram of log TP.

range are spatially independent. Experimental semivariograms were computed using Eq. (3) in four directions (0, 45, 90 and 135°) to reveal anisotropy in the variation. Anisotropy describes directional spatial structures. Due to the limited amount of data pairs available for different directions it was difficult to identify any clear directional trends. Although there is a hydraulic gradient in WCA-2A that extends from the northeastern canal into the west-south direction we could not confirm these trends in the soil TP dataset. Therefore, we proceeded with the omnidirectional fitted semivariogram model. We used a search neighborhood of 7468 m; 1 angular sector; a minimum number of observations of 4 and an optimum number of observations of 10 to predict TP at unsampled locations using OK. The OK prediction map is shown in Fig. 20.5. Based on cross-validation the mean prediction error was −41.77 indicating a slight underestimation of true observations and a root mean square prediction error of 257 mg kg^{-1}. The coefficient of determination (R^2) between measured TP and estimated TP was 0.82 indicating good predictions. To highlight differences between TP

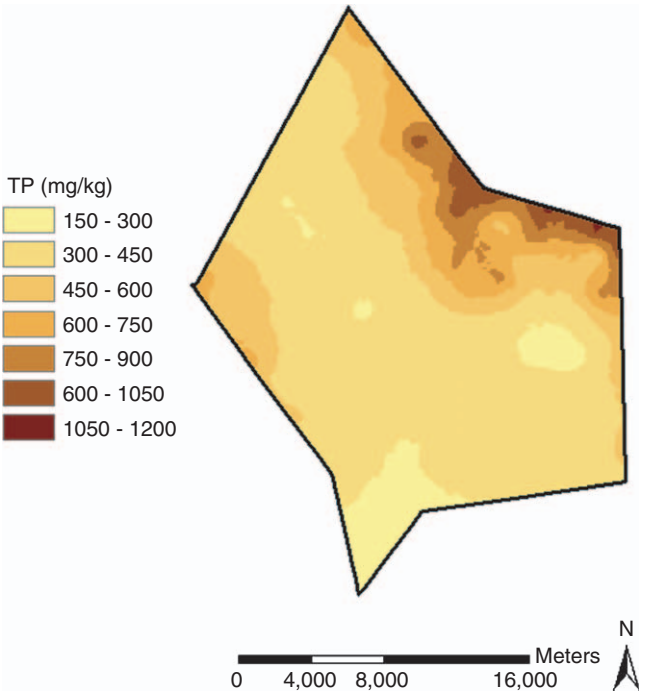

Figure 20.5. Predictions of TP based on Ordinary Kriging.

predictions derived from our spatially distributed observations and observations along a linear corridor (transect) we created a subset of observations extending along a previously identified TP gradient (Reddy et al., 1997; DeBusk et al., 2001). The corridor extended from the hydrologic boundary in the east into the interior of the marsh to the south-west boundary (Fig. 20.6a). Total phosphorus observations were predicted based on 10 observations along the linear corridor using OK. We derived a difference map by subtracting the TP predictions made along the linear corridor from the TP predictions derived from the spatially distributed design (Fig. 20.6b). The difference map shows deviations of more than -240 up to $180\,\mathrm{mg\,kg^{-1}}$ TP illustrating the large differences between both prediction maps. This example illustrates the limitations of sparse biogeochemical datasets based on only 10 observations along a corridor. Sparse datasets along corridors/transects have major limitations to map the underlying spatial variability. In the eastern part of WCA-2A, low TP values (328 and $380\,\mathrm{mg\,kg^{-1}}$) coexisted with very high TP values ($1259\,\mathrm{mg\,kg^{-1}}$) in close proximity (Fig. 20.6b). In contrast, over large distances from the interior of the marsh to the south-west hydrologic boundary, TP values were relatively invariant at different lags ranging from 257 to $371\,\mathrm{mg\,kg^{-1}}$ TP.

Prediction maps are valuable to characterize the spatial distribution and variability of biogeochemical properties such as TP. However, to assess the impact of biogeochemical properties exceeding thresholds that stimulate net productivity and turnover rates is important to characterize the ecological integrity and structure of an ecosystem. Thus, we used IK to derive the probabilities of TP being above a respective cutoff value (z_k) of 450, 500, 550, 600, 650 and $700\,\mathrm{mg\,kg^{-1}}$ (Fig. 20.7). For reference purposes, historical background TP concentrations in WCA-2A have been estimated to be $500\,\mathrm{mg\,kg^{-1}}$ (DeBusk et al., 2001). Probability maps are well suited for decision makers demonstrating the outcome ranging from conservative assumptions (low threshold value) to liberal assumptions (high threshold value). Hot spots can be well identified using IK highlighting the extreme values that exceed the background concentrations.

Stochastic simulations emphasize the uncertainty associated with predictions of biogeochemical properties generating hundreds or thousands of realizations. We used CSGS to generate 100 realizations of TP (Fig. 20.8) using the following modeling options: dilation radius of 20 in the x and y direction; 15 maximum number of data nodes; and 5 maximum number of simulation nodes. The E-type map of the mean showed similar patterns of TP as seen on the OK prediction map. However, the TP patterns in Fig. 20.8 were much more speckled when compared to the

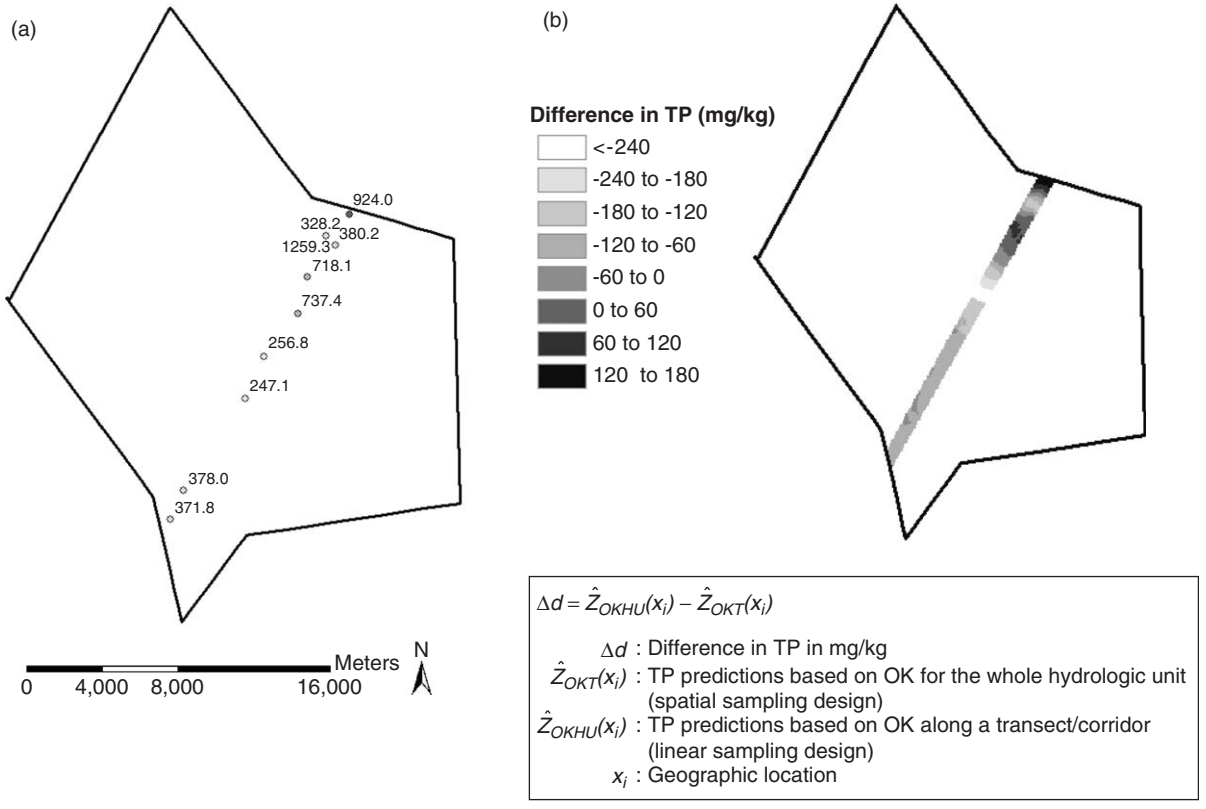

Figure 20.6. (a) Transect/corridor along TP gradient extending from the hydrologic boundary into the marsh interior. Map shows point TP observations in mg kg^{-1}. (b) Map shows the difference in TP predictions along the transect/corridor derived from a spatial and linear sampling design.

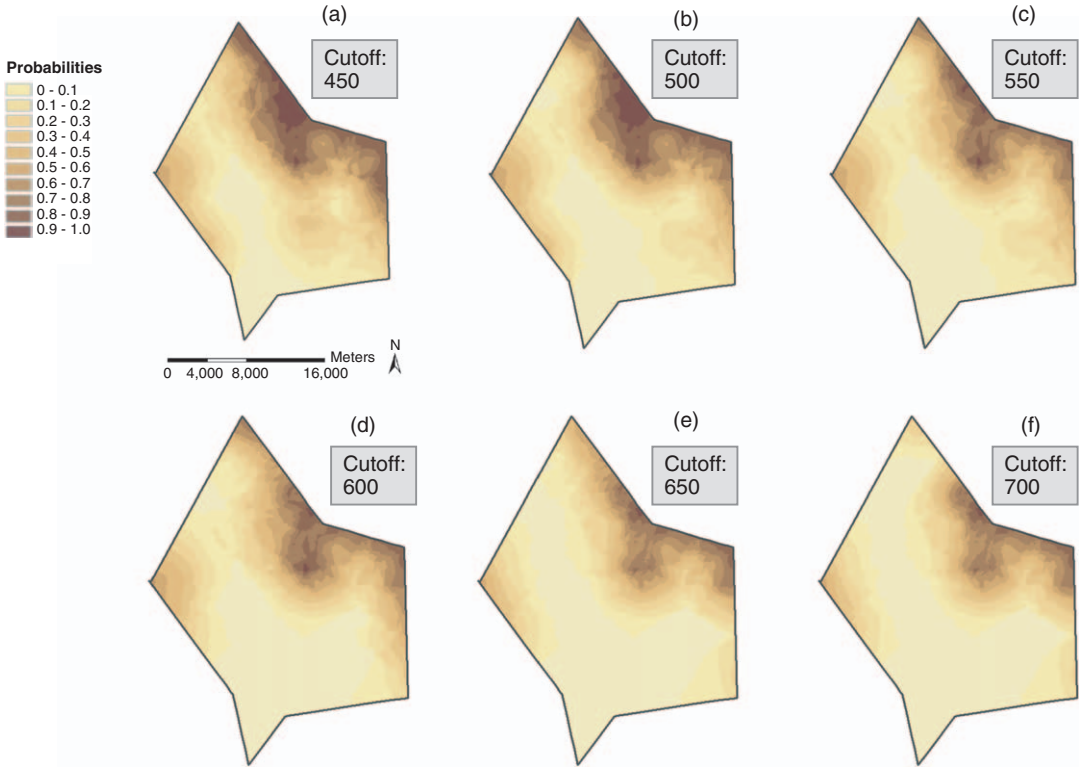

Figure 20.7. Probabilities of being above respective TP cutoff values derived from Indicator Kriging.

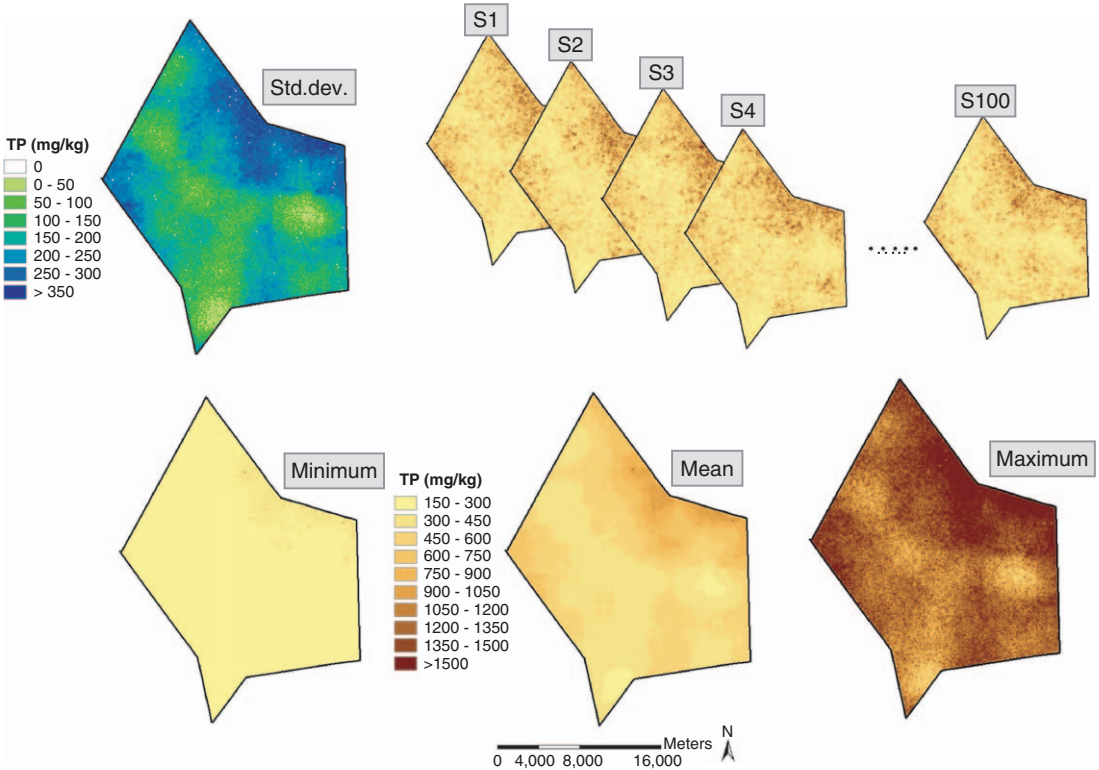

Figure 20.8. Minimum, mean, maximum and select realizations (S1, S2, S3, S4, S5, …, S100) of TP generated with Conditional Sequential Gaussian Simulation. The uncertainty of predictions is expressed by the standard deviation (std. dev.)

smooth OK prediction map. The uncertainty of TP predictions based on CSGS was expressed using minimum and maximum realization maps that show the range of realizations and the standard deviation map. The largest uncertainty was found in the eastern part of WCA-2A coinciding with high TP predictions. The lowest uncertainty was found in the interior of the marsh extending south and eastwards mirroring the lowest observed and predicted TP.

To improve predictions of TP we analyzed the relationships between soil TP, spectral bands and the NDVI. The Spearman Correlation Coefficient (r) between TP and NDVI was high with 0.65. We used a stepwise multiple regression to quantify the relationship between soil and spectral data and derived the following algorithm:

$$\mathrm{TP} = 401.78 + 1890.77 * \mathrm{NDVI} \quad \text{with an } R^2 \text{ of } 0.37\ (p = 0.001)$$

This linear relationship was used as trend model to predict TP across WCA-2A using the exhaustive NDVI pixel dataset. We derived residuals by subtracting the trend model from the observations. The spatially autocorrelated residuals were then kriged and residual predictions added to the global trend model to generate the TP prediction map shown in Fig. 20.9. The RK procedure showed a R^2 of 0.93, which was higher than the one derived for OK (R^2 of 0.82). Overall, the TP prediction map derived from RK showed similar patterns as seen on the OK prediction map (Fig. 20.5) and the CSGS realization maps (Fig. 20.8). However, predictions in Fig. 20.9 highlighted landscape features such as vegetative patterns, slough/ridge systems, open water, tree islands, etc. mapped through the NDVI index that showed quantitative linkages to soil TP. Predictions derived from RK do not honor observed data values and have limitations to describe the uncertainty of predictions. This is the strength of stochastic simulations that are focused to characterize the uncertainty of predictions.

In Fig. 20.10 we contrast the different geospatial methods and TP observations in terms of their distribution functions. Predictions based on RK and realizations derived from CSGS showed the closest match to the distribution of TP observations. In particular, the high TP values above $1050\,\mathrm{mg\,kg^{-1}}$ were well represented in the RK and CSGS maps.

20.4. Remarks

Considering the complexity of wetland ecosystems it is essential to employ spatially distributed sampling designs and geospatial prediction methods that have the ability to characterize the underlying spatial

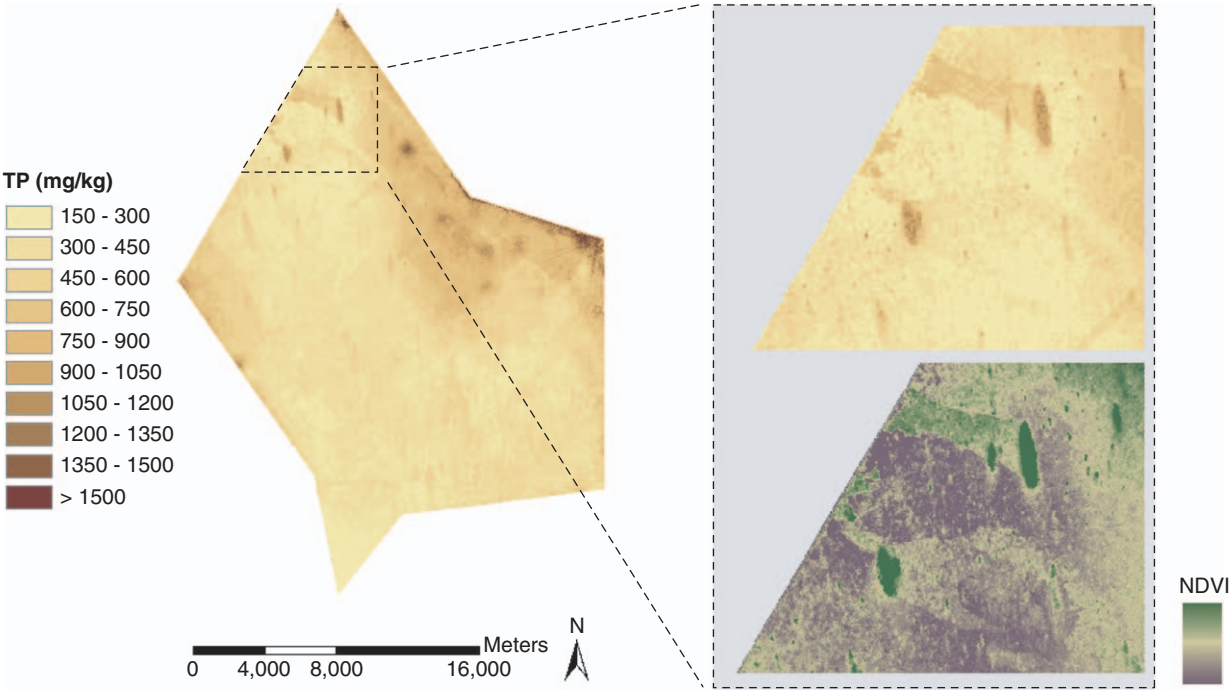

Figure 20.9. Left: Predictions of TP derived from Regression Kriging. Right: Close-up of TP predictions and NDVI map depicting landscape features such as tree islands and vegetation structures.

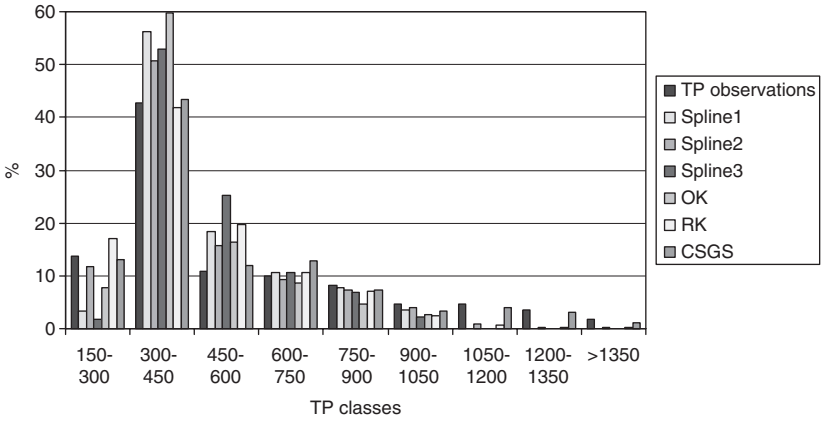

Figure 20.10. Distribution functions of TP observations, predictions and realizations generated with different interpolation methods.

distribution and variability of biogeochemical properties. The integration of sparse point observations of biogeochemical properties and dense ancillary environmental datasets has the potential to improve spatially explicit predictions of properties throughout aquatic (and terrestrial) ecosystems. For example, remote sensing data are cost-effective and provide exhaustive, high-resolution information at landscape-scale. In this chapter we focused on spatially explicit mapping of soil biogeochemical properties exemplified by TP. The case study demonstrated that OK, IK, RK and CSGS produced different maps using the same TP observations. All maps are valid in the sense that they describe the spatial patterns of TP in this specific wetland. Since different geostatistical methods aim at different goals (e.g., to minimize the variance, assess the uncertainty of model predictions, etc.) we have to use them cautiously. Multi-variate geostatistical and hybrid methods that incorporate ancillary environmental data to model biogeochemical properties have much potential to improve our understanding of aquatic and terrestrial ecosystems. To document the evolution of biogeochemical properties through time more monitoring programs are in need. Bridging the gaps between micro, meso and macro spatial scales will be the challenge of future research in aquatic and terrestrial biogeochemistry.

ACKNOWLEDGEMENTS

Funding was provided by the South Florida Water Management District and varied other federal sources. We would like to thank Todd Z.

Osborne (Soil and Water Science Dept, UF), Sue Newman (South Florida Water Management District) and Terry Jones (Aircoastal Helicopter) to assist with data collection; Yu Wang of the Wetland Biogeochemistry Laboratory for her assistance with the laboratory analyses. This research was supported by the Florida Agricultural Experiment Station and approved for publication as Journal Series No. R-10817.

REFERENCES

Abrams, M., Hook, S., Ramachandran, B., 2002. ASTER user handbook. Version 2. Pasadena, CA; Jet Propulsion Laboratory, Sioux Fall, SD, EROS Data Center.

Anderson, J.M., 1976. An ignition method for determination of total phosphorus in lake sediments. Water Res. 10, 329–331.

Berthouex, P.M., Brown, L.C., 2002. Statistics for Environmental Engineers. Lewis, New York, p. 489.

Burrough, P.A., 1986. Principles of geographical information systems for land resources assessment. Clarendon Press, UK, p.194.

Burrough, P.A., McDonnell, R.A., 1998. Principles of geographical information systems—spatial information systems and geostatistics. Oxford University Press, Oxford, UK, p. 333.

Bruland, G.L., Richardson, C.J., 2005. Spatial variability of soil properties in created, restored and paired natural wetlands. Soil Sci. Soc. Am. J. 69, 273–284.

Chilès, J.-P., Allard, D., 2005. Stochastic simulation of soil variations. In: Grunwald, S. (Ed.), Environmental Soil-Landscape Modeling—Geographic Information Technologies and Pedometrics. CRC Press, New York, pp. 289–323.

Chilès, J.-P., Delfiner, P., 1999. Geostatistics—Modeling Spatial Uncertainty. Wiley-Interscience, New York, p. 695.

Craft, C.B., Chiang, C., 2002. Forms and amounts of soil nitrogen and phosphorus across a longleaf pine-depressional wetland landscape. Soil Sci. Soc. Am. J. 66(5), 1713–1721.

DeBusk, W.F., Newman, S., Reddy, K.R., 2001. Spatial and temporal patterns of soil phosphorus in Everglades Water Conservation Area 2A. J. Environ. Qual. 30, 1438–1446.

Fisher, R.A., 1925. Statistical methods for research workers. Oliver and Boyd, Edinburgh, Scotland, p. 189.

Fisher, M.M., Reddy, K.R., 2001. Phosphorus flux from wetland soils affected by long-term nutrient loading. J. Environ. Qual. 30(1), 261–271.

Geary, R.C., 1954. The contiguity ratio and statistical mapping. Incorporated Statistician 5, 115–145.

Goovaerts, P., 1997. Geostatistics for natural resources evaluation. Oxford University Press, New York, p. 483.

Goovaerts, P., 1999. Geostatistics in soil science: State-of-the-art and perspectives. Geoderma 89, 1–45.

Grunwald, S., 2005. What do we really know about the space-time continuum of soil-landscapes?. In: Grunwald, S. (Ed.), Environmental Soil-Landscape Modeling—Geographic Information Technologies and Pedometrics. CRC Press, New York, pp. 3–37.

Grunwald, S., Corstanje, R., Weinrich, B.E., Reddy, K.R., 2006. Spatial patterns of labile forms of phosphorus in a subtropical wetland 10 years after a sustained nutrient impact. J. Environ. Qual. 35, 378–389.

Grunwald, S., Reddy, K.R., Newman, S., DeBusk, W.F., 2004. Spatial variability, distribution and uncertainty assessment of soil phosphorus in a south Florida wetland. Environmetrics 15, 811–825.

Hengl, T., Heuvelink, G.B.M., Stein, A., 2004. A generic framework for spatial prediction of soil variables based on regression-kriging. Geoderma 120, 75–93.

Holling, C.S., Gunderson, L.H., 2002. Resilience and adaptive cycles. In: Gunderson, L.H., Holling, C.S. (Eds.), Panarchy: Understanding Transformations in Human and Natural Systems. Island Press, Washington, D.C., p. 287.

Isaaks, E.H., Srivastava, R.M., 1989. An introduction to applied geostatistics. Oxford University Press, New York, p. 289.

Karathanasis, A.D., Thompson, Y.L., Barton, C.D., 2003. Long-term evaluations of seasonally saturated wetlands in western Kentucky. Soils Sci. Soc. Am. J. 67(2), 662–673.

Levin, S.A., 1992. The problem of pattern and scale in ecology. Ecology 73, 1943–1967.

McBratney, A.B., Odeh, I.O.A., Bishop, T.F.A., Dunbar, M.S., Shatar, T.M., 2000. An overview of pedometric techniques for use in soil survey. Geoderma 97, 293–327.

McBratney, A.B., Mendonça Santos, M.L., Minasny, B., 2003. On digital soil mapping. Geoderma 117, 3–52.

McCollum, S.H., Carlisle, V.W., Volk, B.G., 1976. Historical and current classification of organic soils in the Florida Everglades. Proc. Soil Crop Sci. Soc. FL 35, 173–177.

McCormick, P.V., Newman, S., Miao, S., Gawlik, D., Marley, D., Reddy, K.R., Fontaine, T., 2002. Effects of anthropogenic phosphorus inputs on the Everglades. In: Porter, J.W., Porter, K.G. (Eds.), The Everglades, Florida Bay, and Coral Reefs of the Florida Keys: An Ecosystem Sourcebook. CRC Press, Boca Raton p. 1000.

Mitsch, W.J., Gosselink, J.G., 2000. Wetlands. Wiley, New York, p. 920.

Moran, P.A.P., 1950. Notes on continuous stochastic phenomena. Biometrika 37, 17–23.

Morris, D.R., Glaz, B., Daroub, S.H., 2004. Organic matter oxidation potential determination in a periodically flooded Histosol under sugarcane. Soil Sci. Soc. Am. J. 68, 994–1001.

Newman, S., Reddu, K.R., DeBusk, W.D., Wang, Y., Shih, G., Fisher, M.M., 1997. Spatial distribution of soil nutrients in a northern Everglades marsh: Water Conservation Area 1. Soil Sci. Soc. Am. J. 61, 1275–1283.

Noe, G.B., Childers, D.L., Jones, R.D., 2001. Phosphorus biogeochemistry and the impact of phosphorus enrichment: Why is the Everglades so unique. Ecosystems 4, 603–624.

Odeh, I.O.A., McBratney, A.B., 2000. Using AVHRR imageries for spatial prediction of clay content in the lower Namoi Valley of Eastern Australia. Geoderma 97, 237–254.

Odeh, I.O.A., McBratney, A.B., Chittleborough, D.J., 1994. Spatial prediction of soil properties from landform attributes derived from a digital elevation model. Geoderma 63, 197–214.

Odeh, I.O.A., McBratney, A.B., Chittleborough, D.J., 1995. Further results on prediction of soil properties from terrain attributes: Heterotopic cokriging and regression-kriging. Geoderma 67, 215–226.

Porter, J.W. and K.G. Porter, (Eds.), 2002, The Everglades, Florida Bay and Coral Reefs of the Florida Keys—An Ecosystem Sourcebook. CRC Press, New York p. 1000.

Reddy, K.R., Wang, Y., DeBusk, W.F., Fisher, M.M., Newman, S., 1998. Forms of soil phosphorus in selected hydrologic units of Florida Everglades ecosystems. Soil Sci. Soc. Am. J. 62(4), 1134–1147.

Reddy, K.R., White, J.R., Wright, A., Chua, T., 1997. Influence of phosphorus loading on microbial processes in the soil and water column of wetlands. In: Reddy, K.R., O'Connor, G.A., Schelske, C.L. (Eds.), Phosphorus Biogeochemistry in Subtropical Ecosystems. Lewis, New York, p. 707.

Rouse, J.W., Haas, R.H., Schell, J.A., Deering, D.W., 1974. Monitoring vegetation systems in the Great Plains with ERTS. Proceedings, third Earth Resources Technology Satellite-1 Symposium, Greenbelt: NASA SP-351, pp. 3010–3017.

Turner, M.G., O'Neill, R.V., Gardner, R.H., Milne, B.T., 1989. Effects of changing spatial scale on the analysis of landscape pattern. Landscape Ecol. 3(3/4), 153–162.

U.S. Environmental Protection Agency, 1993. Methods for determination of inorganic substances in environmental samples. Environmental Monitoring Systems Lab, Cincinatti, OH, USA.

Webster, R., 1994. The development of pedometrics. Geoderma 62, 1–15.

Webster, R., Oliver, M.A., 2001. Geostatistics for environmental scientists. Wiley, New York, p. 271.

Webster, R., Oliver, M.A., 2005. Modeling spatial variation of soil as random functions. In: Grunwald, S. (Ed.), Environmental Soil-Landscape Modeling Geographic Information Technologies and Pedometrics. CRC Press, New York, pp. 241–289.

White, J.R., Reddy, K.R., 2000. Influence of phosphorus loading on organic nitrogen mineralization of Everglades soils. Soil Sci. Soc. Am. J. 64(4), 1525–1534.